SUPPORTING INFORMATION

Building depletion-region width modulation model, realizing memory characteristics in pn heterostructure devices

Xing Guo[#], Xinmiao Li[#], Ruixiao Wang, Wenhui Zhu, Liancheng Wang, Lei Zhang*

Dr. L. Zhang, *X. Guo*, *X. M. Li*, *Prof. W. H. Zhu*, *Prof. L. C. Wang*

State Key Laboratory of High Performance Complex Manufacturing, College of Mechanical and Electrical Engineering, Central South University, Changsha, 410000, China

[#] The authors contributed equally to this work.

Corresponding Author: Lei Zhang; zhangl207@csu.edu.cn

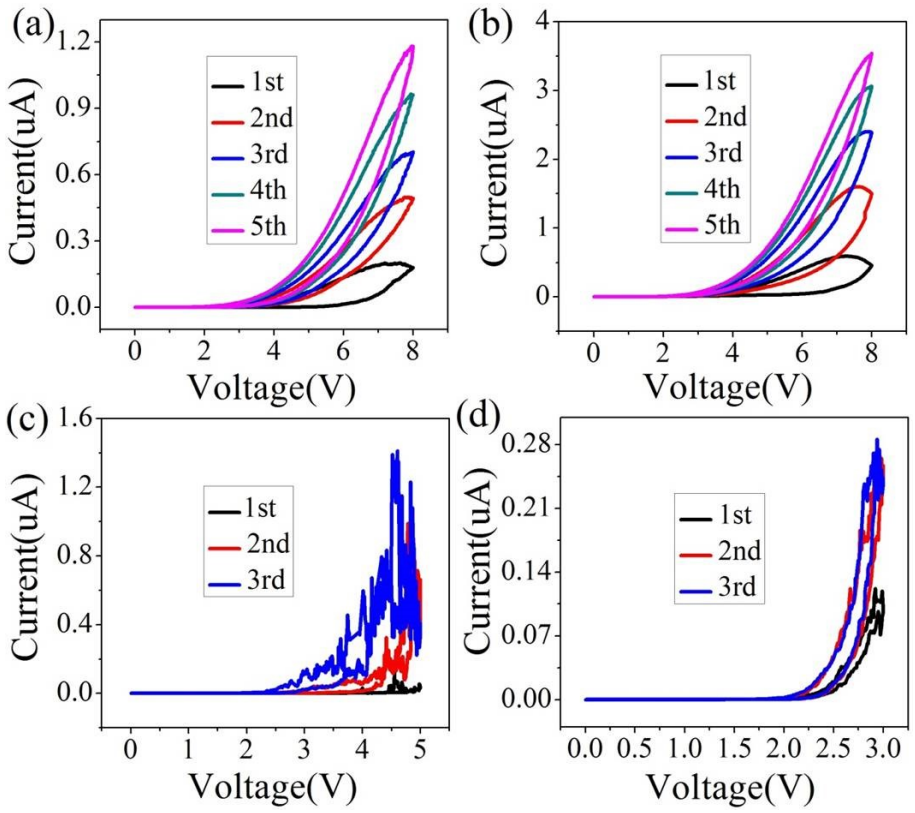

Supplementary Figure S1 The effect of film thickness on the memristive behavior. (a) Pt/80nm-$CuAlO_2$/40nm-ZnO/Pt and (b) Pt/80nm-$CuAlO_2$/20nm-ZnO/Pt show obvious memristive behaviors when decreases the thickness of ZnO film. The stable memristive behaviors disappear in the (c) Pt/40nm-$CuAlO_2$/80nm-ZnO/Pt and (d) Pt/20nm-$CuAlO_2$/80nm-ZnO/Pt device when decease the thickness of $CuAlO_2$ film. Compared with the majority carrier density of p-$CuAlO_2$ and n-ZnO, the depletion region is mainly located in the p-$CuAlO_2$ side. The devices with the decreasing thickness of $CuAlO_2$ film may decrease the effective depletion region width, affecting the memristive behaviors. All of them indicate that the memristive behaviors are more depended on the $CuAlO_2$ layer, in other words the depletion region width.

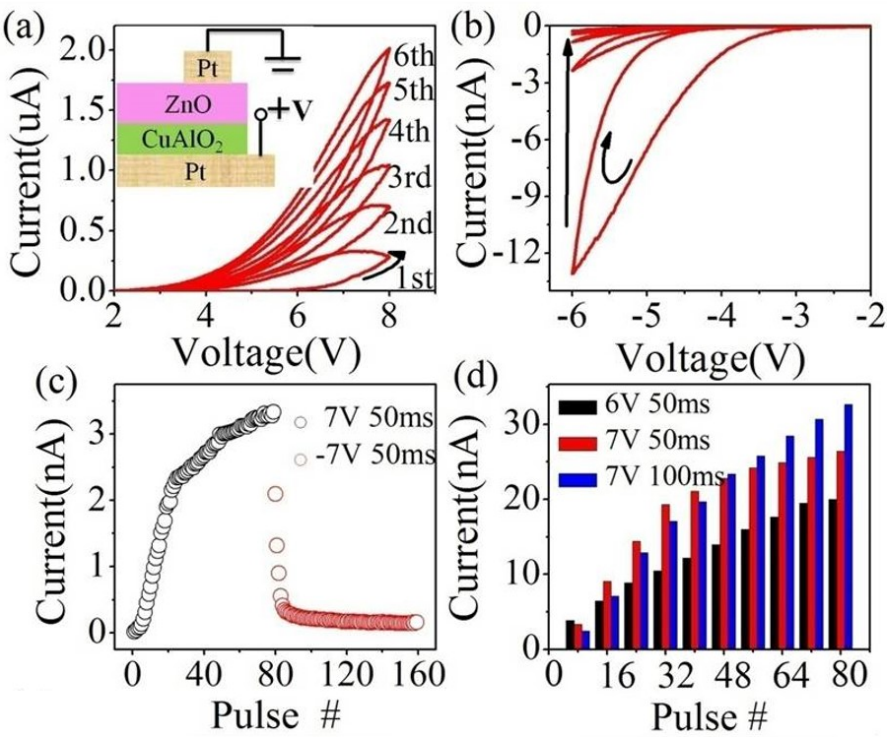

Supplementary Figure S2 The coexistence of memristive and memcapacitive characteristics in Pt/p-$CuAlO_2$/n-ZnO/Pt heterostructure device. (a) and (b) show the I-V characteristics of Pt/$CuAlO_2$/ZnO/Pt memristor (inset) with the applied positive and negative voltages in double sweep model, respectively. The device conductivity continuously increases (decreases) during positive (negative) voltage sweeps. (c) The change of device conductivity has also been exhibited by consecutive positive (negative) pulses. (d) Higher-amplitude and longer-duration pulses cause a larger change in device conductivity.

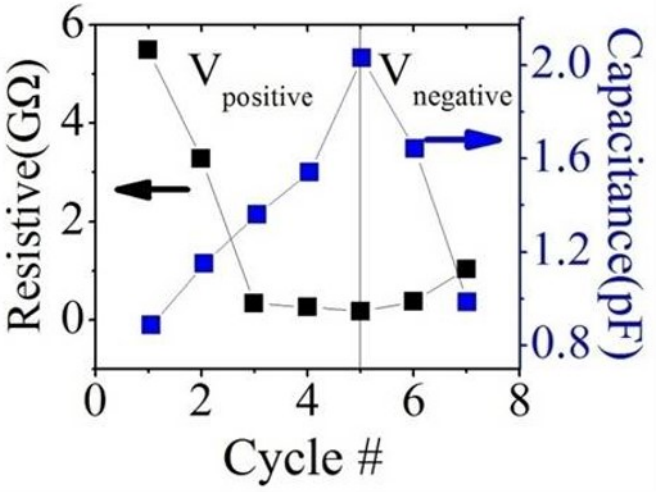

Supplementary Figure S3 The gradual variation of resistance and capacitance with positive and negative double voltage sweeps. These results indicate that the Pt/p-$CuAlO_2$/n-ZnO/Pt heterostructure device realizes the coexistence of memristive and memcapacitive characteristics.

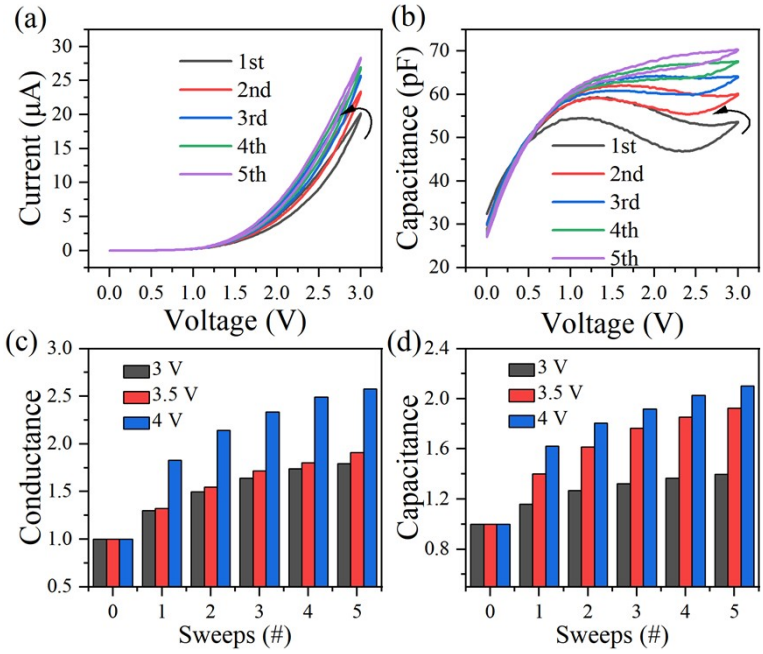

Supplementary Figure S4 The coexistence of memristive and memcapacitive characteristics in p^+-Si/ZnO/Ni heterostructure device. (a) and (b) show the I-V and C-V characteristics of p^+-Si/ZnO/Ni memristor with the applied positive and negative voltages in double sweep model, respectively. The device's conductivity continuously increases during positive voltage sweeps. (c) and (d) The change in

device conductivity and capacitance under consecutive positive sweeps at different biases.

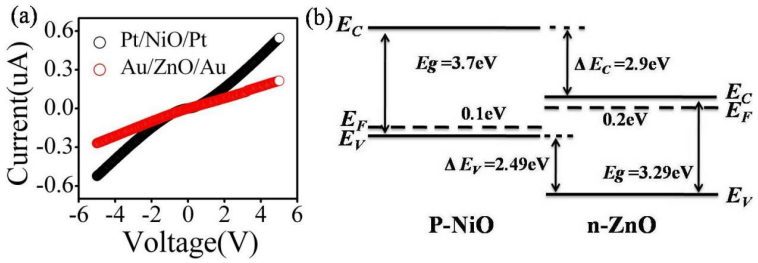

Supplementary Figure S5 The study of p-NiO/n-ZnO heterojunction.(a) The I-V cures of Pt/NiO/Pt and Au/ZnO/Au reference devices. This reference devices exhibit the symmetric and nearly linear I-V characteristic, which indicates that the metal materials (Pt and Au) can effectively eliminate the Schottky barrier between electrode and dielectric layer. (b) The energy band of p-NiO/n-ZnO heterojunction. When p-NiO material comes into contact with n-ZnO material, the electron will diffuse from ZnO to NiO and the hole will diffuse from NiO to ZnO owing to the difference of Fermi level. The depletion region will appear at the interfaces, and the direction of built-in electric field should be from ZnO to NiO.

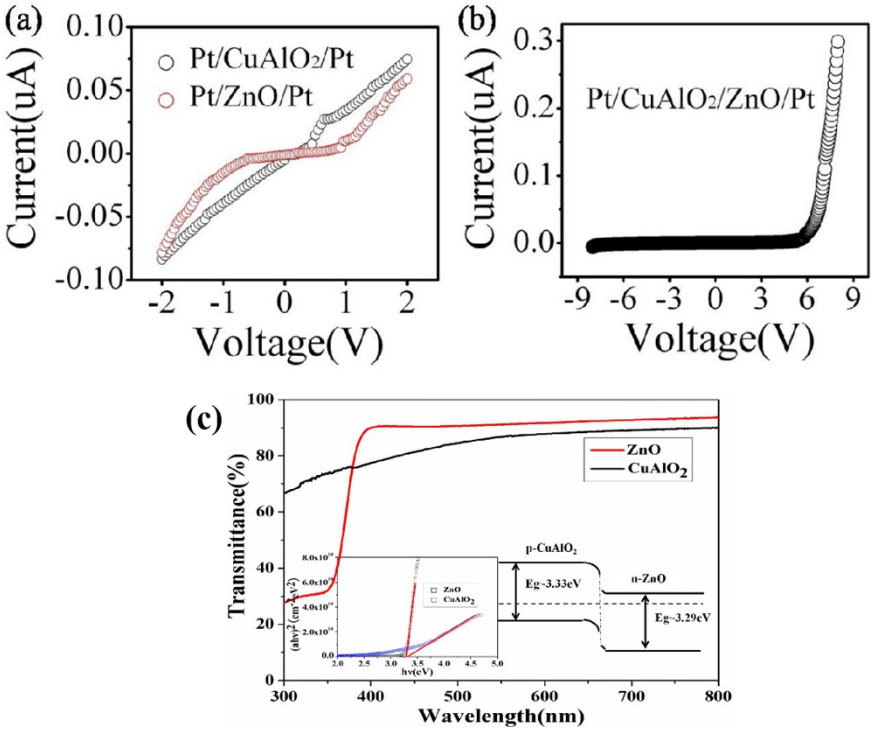

Supplementary Figure S6 The study of p-$CuAlO_2$/n-ZnO heterojunction. (a) The I-V cures of Pt/$CuAlO_2$/Pt and Pt/ZnO/Pt reference devices. (b) The nonsymmetric rectifying I-V cure of Pt/$CuAlO_2$/ZnO/Pt heterostructure device. The reference devices exhibit the symmetric I-V curves or smaller junction resistance compared with the Pt/$CuAlO_2$/ZnO/Pt device. The rectifying characteristic is mainly source from $CuAlO_2$/ZnO heterojunction. (c) Optical transmission spectra of ZnO and $CuAlO_2$ thin films. The forbidden bandwidth and energy band of p-$CuAlO_2$/n-ZnO heterojunction in the inset. The depletion region appears at the $CuAlO_2$/ZnO interface, and the direction of built-in electric field is from ZnO to $CuAlO_2$.

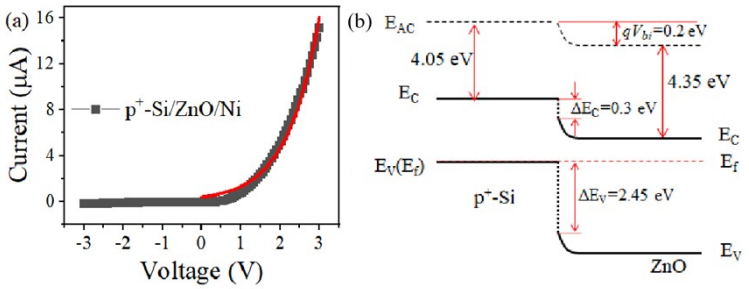

Supplementary Figure S7 The study of p^+-Si/n-ZnO heterojunction. (a) The nonsymmetric rectifying I-V curve of p^+-Si/n-ZnO/Ni heterostructure device. The rectifying characteristic is mainly source from p^+-Si/n-ZnO/Ni heterojunction. (b) The

energy band of p^+-Si/n-ZnO heterojunction. The depletion region appears at the p^+-Si/n-ZnO interface, and the direction of built-in electric field is from n-ZnO to p^+-Si.

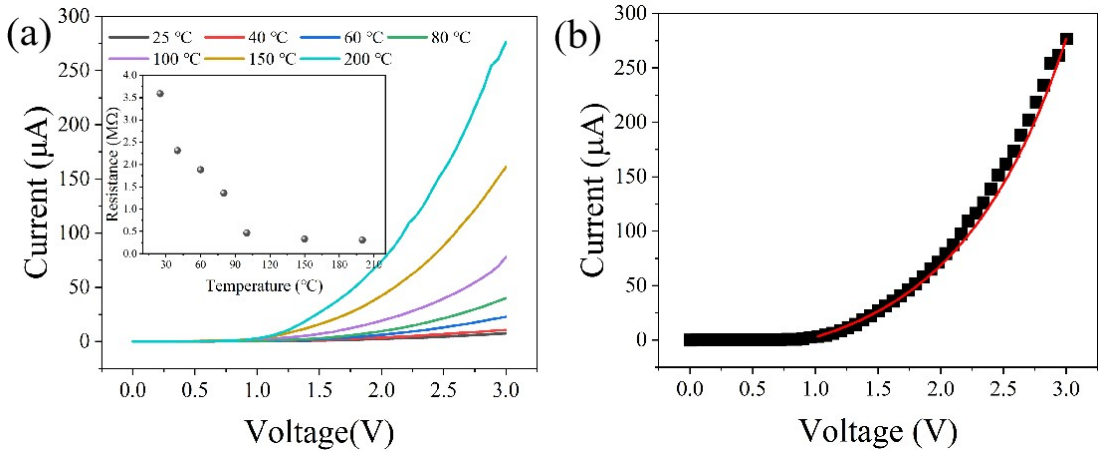

Supplementary Figure S8 Electrical measurements of p^+-Si/n-ZnO heterojunctions at different temperatures. (a) The I-V curves of the device at different temperature tests have been given in figure. The device resistance at different test temperatures is given in the inset of the figure. The resistance of the device increases with increasing test temperature. **(b)** I-V curves at 200 ℃ test temperature can be fitted by the equation: $J=J_s[\exp(qV/kT)-1]$, J is the total current density, J_s is the reverse saturation current, q is the charge density, V is the applied voltage, k is the Boltzmann constant, and T is the temperature.

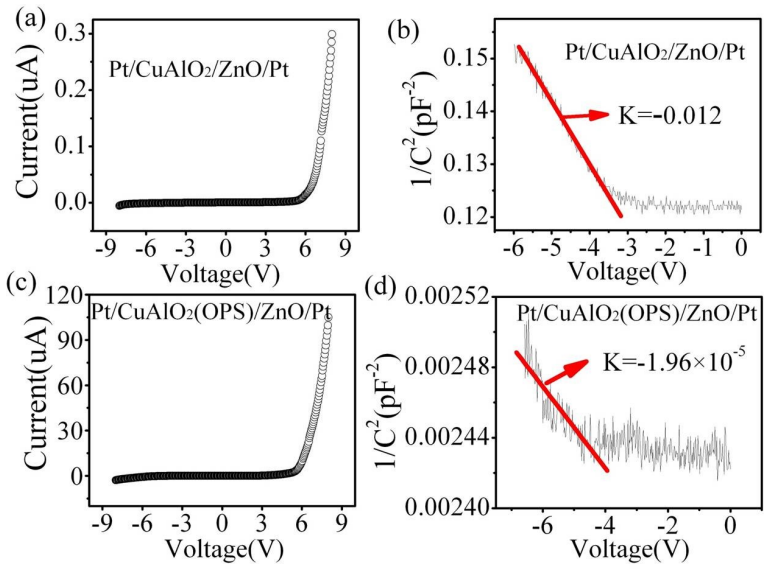

Supplementary Figure S9 The electrical property of Pt/$CuAlO_2$/ZnO/Pt and oxygen plasma sputtering (OPS) processed Pt/$CuAlO_2$/ZnO/Pt devices. (a) and (b) show I-V and C^{-2}-φ curves of Pt/$CuAlO_2$/ZnO/Pt device, respectively. (c) and (d) show I-V and C^{-2}-φ curves of OPS processed Pt/$CuAlO_2$/ZnO/Pt device, respectively. A linear dependence has been obtained by C^{-2}-φ (Mott-Schottky) plot. For pn heterostructure device, the donor density can be obtained from the slope $dC^{-2}/d\varphi=-2/q\varepsilon_0\varepsilon_r N_D A^2$. Here, q is the elementary charge, ε_0 is the vacuum permittivity, ε_r the relative dielectric constant of semiconductor layer, and A the surface area of the contact. As is well-known, $CuAlO_2$ as a p-type semiconductor material, the OPS operation can increase the carrier concentration (Cu vacancy concentration) of $CuAlO_2$ surface. The slope of Mott-Schottky plot in **Fig. S9**d is smaller than that in **Fig. S9**b. The OPS method can effectively increase the carrier concentration, decreasing the depletion region width. Meanwhile, the nonsymmetric rectifying I-V curve shows better conductivity for OPS processed device. We find that the device with the decreased depletion-region width has the higher device conductivity, proving the proposed depletion-region width modulation model.

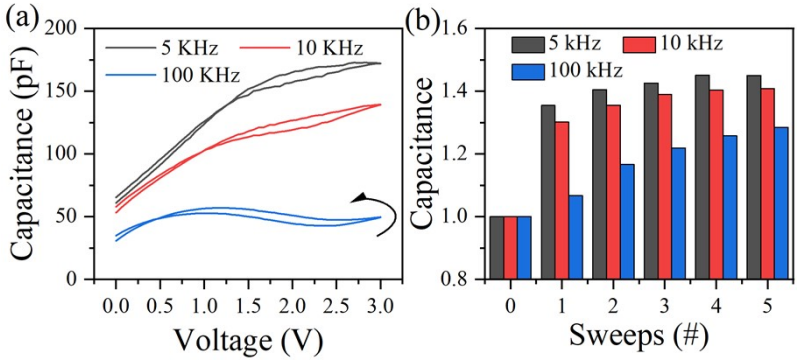

Supplementary Figure S10 The change of p^+-Si/ZnO/Ni device capacitance has also been exhibited by consecutive positive sweeps at different frequency.

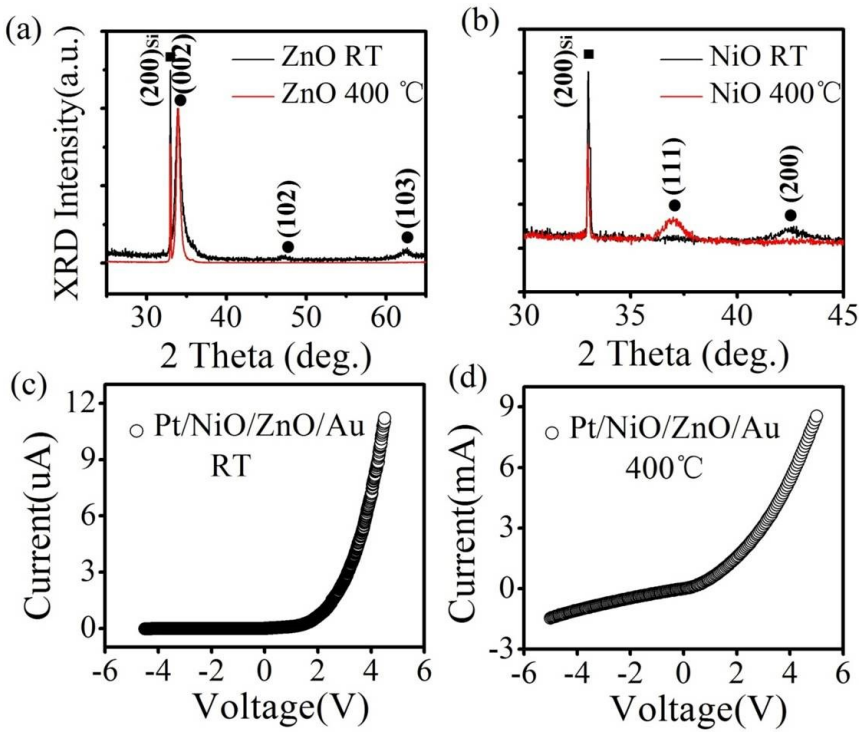

Supplementary Figure S11 The effect of crystallinity on memristive and memcapacitive behaviors. (a) and (b) show the XRD pattern of RT- and 400℃-deposited ZnO and NiO film, respectively. (c) and (d) The I-V cures of RT- and 400℃-deposited Pt/NiO/ZnO/Au devices, respectively. The 400℃-deposited ZnO film achieves the better crystallization quality with a c-axis (002) orientation of hexagonal structure, while the RT-deposited ZnO film exhibits relative inferior quality with relatively stronger (002) peak and weaker (102) (103) peaks in **Fig. S11**a. The 400℃ and RT-deposited NiO films respectively exhibit the (111) and (200) orientation of cubic structure in **Fig. S11**b. The 400℃-deposited NiO film shows the narrower half-peak breadth than the RT-deposited NiO film. For the 400 ℃-deposited device, the cubic NiO (111) orientation and hexagonal ZnO (002) orientation show small lattice mismatch and have the good epitaxial relationships. The small bias voltage will turn-on pn junction in **Fig. S11**d. However, the RT-deposited device has smaller current than the 400℃-deposited device (about 3 order of magnitudes), illustrating that the RT-deposited device exist lots of defect states (unstable and metastable local oxygen ions or oxygen vacancy) due to the rough film quality. It will lead to a broadening depletion-region width for the RT-deposited pn heterostructure device.

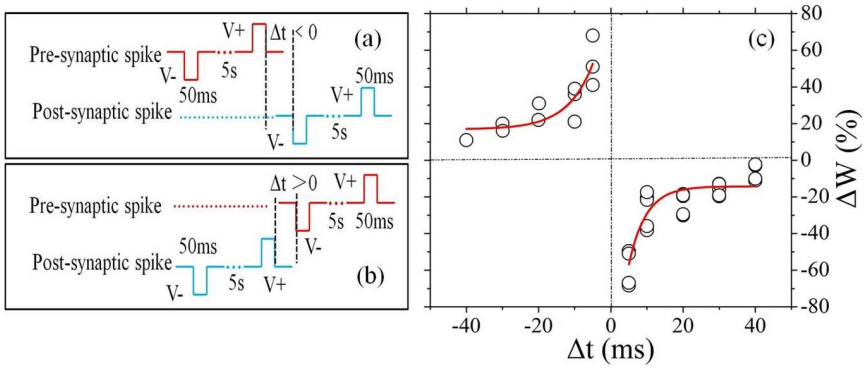

Supplementary Figure S12 The demonstration of STDP in Pt/CuAlO$_2$/ZnO/Pt heterostructure memristor. (a) and (b) A pair of the pre- and post-synaptic spikes, which are designed to implement STDP. (c) The relative change of the memristor synaptic weight (ΔW) versus the relative spike timing (Δt). The solid lines are the exponential fits to the experimental data. The fitting results show typical STDP characteristics of biological synapses.

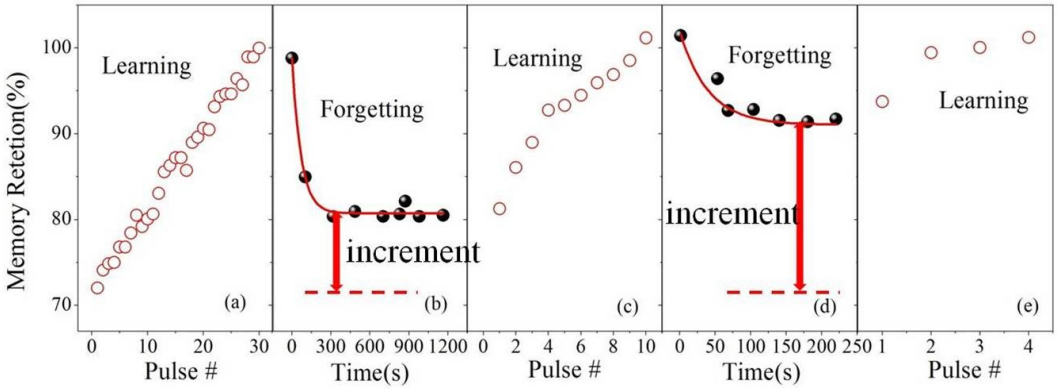

Supplementary Figure S13 The Long-Term/Short-Term Plasticity (LTP/STP) and "learning-experience" behaviors. (a) Nearly linear increase of the device conductivity with the consecutive stimuli. (b) and (d) The spontaneous decay of the conductivity, that is, the relaxation process of STP. The memory absolute value is incremental through continuous learning. (c) and (e) Re-stimulation process from the mid-state. The less numbers of stimuli are required to make the device recover its memory than that for the first learning process, which bears striking resemblance to the learning process based on experience for biological systems.

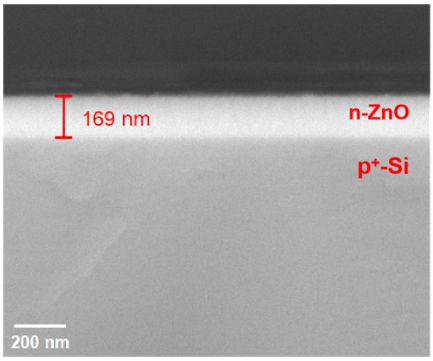

Supplementary Figure S14 The cross sectional image of p^+-Si/ZnO layer using scanning electron microscopy (SEM).